Improved light transmission for III-V lasers monolithically integrated on Si platforms

Michele Paparella, Andres Remis, Marco Grande, Thierry Taliercio, Laurent Cerutti, Jean-Baptiste Rodriguez, Eric Tournié

Research Article | Vol. 32, No. 22 / 21 Oct 2024 / Optics Express 38994

Optics EXPRESS

Improved light transmission for III-V lasers monolithically integrated on Si platforms

MICHELE PAPARELLA,[1,2,3] ANDRES REMIS,[1,4] MARCO GRANDE,[2] THIERRY TALIERCIO,[1] LAURENT CERUTTI,[1] JEAN-BAPTISTE RODRIGUEZ,[1] AND ERIC TOURNIÉ[1,5,*]

[1]*IES, University of Montpellier, CNRS, F-34000 Montpellier, France*
[2]*Polytechnic University of Bari, IT-70126 Bari, Italy*
[3]*Currently with Optoelectronics Research Centre, University of Southampton, SO17 1BJ Southampton, UK*
[4]*Currently with C2N, CNRS, University Paris-Saclay, F-91120 Palaiseau, France*
[5]*Institut Universitaire de France (IUF), F-75005 Paris, France*
[*]*eric.tournie@umontpellier.fr*

Abstract: We propose a strategy to monolithically integrate active III-V lasers and passive dielectric devices, where the passive waveguides are fabricated after the MBE growth of the III-V semiconductors on a planar Si substrate. This avoids any airgap at the active/passive interface, replaced by a thin dielectric interface layer which improves the light coupling efficiency. We demonstrate GaSb DLs butt-coupled to SiN waveguides with ~23% transmission after 2 mm SiN, corresponding to ~35% transmission at the active/passive interface. We propose several routes to further increase the transmission factor. This strategy eliminates the need for trenches or pockets, which have been shown to cause poor quality material near the dielectric stack facet and to affect the laser lifetime. This strategy thus paves the way for an optimized route to monolithically integrate active and passive photonic devices with a high light coupling efficiency.

1. Introduction

In the last two decades, silicon (Si) photonics has emerged as the main technology for realizing photonic integrated circuits (PICs), with high performance Si PICs demonstrated for data/telecom applications as well as for on-chip sensors [1,2]. However, despite various efforts to develop group-IV-based active devices, Si is not suitable for light emission [3] and III-V semiconductors remain the most efficient materials for fabricating on-chip light sources. Their integration on Si wafers is a key building block to enable active Si-based PICs. Today, integration techniques based on the bonding of III-V devices on Si substrates or PICs - also commonly known as hybrid or heterogeneous integration [4]- are the most mature and widely used approaches. Based on an evanescent coupling geometry, light can be efficiently coupled into Si-based waveguides [5–7]. However, low integration density, III-V material waste and high fabrication cost limit the efficiency of these options. Among bonding technologies, micro-transfer printing appears to be the best compromise for improving the integration density and III-V material utilization yield [8].

In addition, much research effort is also focused on another approach, the direct epitaxy of III-V heterostructures on Si, a scenario known as monolithic integration. This technique is expected to greatly increase the on-chip light source density and offers the highest efficiency of the III-V material utilization, allowing the realization of low-cost and more environmentally friendly PIC devices [9]. However, the direct epitaxy of III-V materials on a Si substrate is plagued by structural defects such as antiphase domains (APDs) and threading dislocations (TDs), which degrade the performance of the devices. Although these defects cannot be avoided, growth strategies have been developed to mitigate their effects [10,11]. However, they result in thick

#537703 https://doi.org/10.1364/OE.537703
Journal © 2024 Received 26 Jul 2024; revised 23 Sep 2024; accepted 30 Sep 2024; published 11 Oct 2024

Optics EXPRESS

buffer layers (> 1 μm) that preclude evanescent coupling. In this case, butt coupling appears as a possible coupling approach, and recent reports have indeed shown that the light emitted by III-V diode lasers (DLs) grown on Si substrates can be successfully butt-coupled into passive waveguides (WGs) [12–14]. In these demonstrations, Si or Si_3N_4 waveguides were first patterned on Si wafers and recesses were opened to expose the Si substrate for subsequent III-V growth by molecular beam epitaxy (MBE). The III-V gain materials were then processed on-chip to form the DLs. However, such a process flow inevitably leads to the formation of an airgap at the interface between the active III-V DLs and the passive WGs, the origin of which is described in detail in Refs. [12–15]. This airgap, in turn, dramatically reduces the light coupling efficiency [15]. In addition, DLs grown in deep and narrow pockets appear to exhibit degraded performance as compared to their counterparts grown on bare Si substrates [16].

In this work, we first investigate the influence of filling the gap for the on-chip PIC studied in [12], in order to observe a potential improvement of the light coupling and to understand the influence of having a coated facet on the laser performance. Based on the experimental measurements obtained by filling the gap, we then propose and demonstrate an alternative strategy to monolithically integrate active and passive devices with the aim of improving the optical coupling. As a case study, we have chosen to integrate a GaSb-based DL designed to emit near 2.3 μm, a wavelength of particular interest for gas sensing such as CH_4, with a Si_3N_4 passive waveguide - a CMOS-compatible material - with remarkable properties such as wide transparent wavelength window, excellent thermal stability, ultra-low loss properties, high Q-factor resonator, to name but a few [17–20].

2. Strategies for improving the optical coupling in a monolithically integrated scenario

In the monolithic integration approaches presented in Refs. [12–14], the laser sources are separated from the passive WGs by an airgap, which arises from the fact that the passive devices are fabricated before the epitaxial growth of the active III-V heterostructure. A careful numerical analysis of the problem shows that the airgap significantly affects the efficiency of light transmission, and that filling the gap with a high index material should improve the optical coupling [15]. In this work, we explore two different approaches. The first is based on filling the airgap between the active and passive interfaces based on the PIC studied in [12]. The second approach, building on the experimental results obtained by filling the gap, proposes an optimized butt coupling geometry that open new routes for improving the light transmission of monolithically integrated on-chip light sources.

2.1. Filling the airgap between the passive and active WGs

The mitigation of insertion losses due to the presence of an air gap at the DL/WG interface is the main problem that can be overcome by filling the gap with a high-index material. More specifically, this approach is expected to reduce the beam divergence before the light couples into the WG. In fact, the beam diverges as a half-angle cone (θ) according to the following relationship [21]:

$$\theta = \frac{\lambda_0}{\pi w_0 n}$$

Where λ_0 is the wavelength in the free space, w_0 waist of the beam and n the refractive index in the medium where light diverges. Therefore, θ decreases as n increases.

A number of materials transparent near 2.3 μm have been considered in [15]. Among possible fillers, a:Si offers a significant improvement in coupling efficiency, favored by the similarity of the refractive index of a:Si and the effective index of the fundamental mode supported by the DL ridge [15]. On the other hand, if a:Si is the best choice for improving the optical coupling [15],

Optics EXPRESS

the laser performance may be adversely affected due to a decrease in cavity mirror reflectivity. In fact, the threshold current density of a laser depends on the mirror loss term α_m, as follows [22]:

$$J_{th} = J_{tr} \exp\left(\frac{\alpha_i + \alpha_m}{N_w \Gamma_w g_0}\right)$$

Where J_{tr} is the transparency current density, N_w is the number of quantum wells (QWs), Γ_W is the mode overlap with the QWs, g_0 is the gain parameter, α_i and α_m the material and mirror losses, respectively. In turn, the mirror loss term is defined as:

$$\alpha_m = \frac{1}{2L} \ln\left(\frac{1}{R_1 R_2}\right)$$

Where L is the length of the cavity, R_1 is the reflection coefficient calculated at the air-coated back facet of the cavity, while R_2 is the reflection coefficient calculated at the interface between the DL facet and the material that fills the gap. Both reflection coefficients are derived from the Fresnel reflection coefficient for the case of normal incidence as follows:

$$R = \left|\frac{n_1 - n_2}{n_1 + n_2}\right|^2$$

Based on a theoretical gain model previously developed for GaSb diode lasers grown on Si [23], the impact of the refractive index of the gap filler on the threshold current density was calculated for a 2 QW GaSb DL grown on Si (Fig. 1) [24].

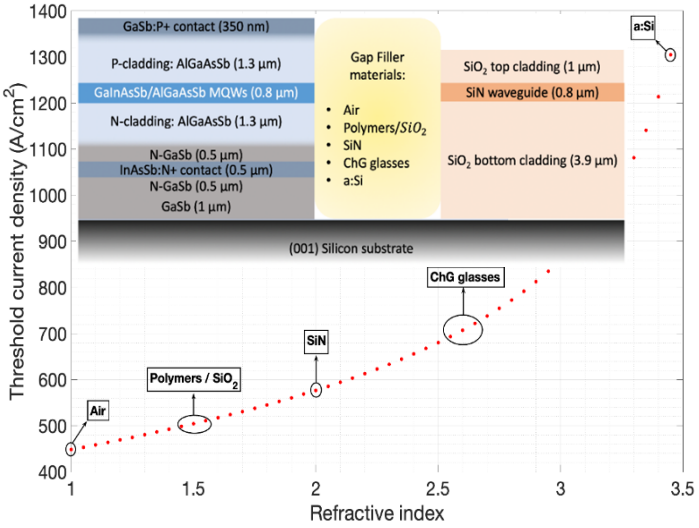

Fig. 1. Threshold current density of a 2 QW GaSb DL grown on Si as a function of the refractive index of the gap filler material, for a 1.5 mm cavity length.

The threshold current density increases from 470 to 510, 590, 720 and 1310 A/cm^2 when the gap is filled with polymers/SiO_2, SiN, chalcogenide (ChG) glasses and a:Si, respectively (Fig. 1). It is worth noting that these calculations were made considering an uncoated back facet. The deposition of a high-reflectivity (HR) coating on the back facet of the laser is an option to increase the reflectivity of the back facet, and thus somehow mitigate the increase of the threshold current. Filling the gap with a:Si (n = 3.44) would thus largely affect the threshold current, making the device inoperable for practical purposes. In addition, it could potentially create shorts on the

Optics EXPRESS

laser facet and, from a manufacturing point of view, the deposition of a:Si in deep trenches may prove difficult and result in a non-conformal distribution [15].

The simulations show that the coupling is improved when the gap is filled with higher index materials. However, it is important to consider whether filling the gap with these materials is feasible from a fabrication standpoint. For materials such as a:Si or chalcogenides, filling a narrow gap may prove cumbersome, so we decided to perform a proof of concept by using a polymer, the polymethylmethacrylate (PMMA), with a refractive index close to 1.47 [25], although the expected improvement in light coupling is lower than for a:Si [15]. In fact, PMMA is a liquid that is easy to handle prior to polymerization, has a refractive index close to that of SiO_2, and does not cause a short circuit in the device because it is insulating. First, the optical properties of PMMA in the mid-IR were evaluated by Fourier Transformed InfraRed (FTIR). Absorption measurement confirmed the transparency of PMMA near 2.3 µm (Fig. 2). As-deposited PMMA exhibits a significant absorption in the wavelength range between 2 and 5 µm, whereas the transmittance measured at $\lambda = 2.3\ \mu m$ after curing the PMMA, and thus after solvent evaporation, is close to 97% (Fig. 2).

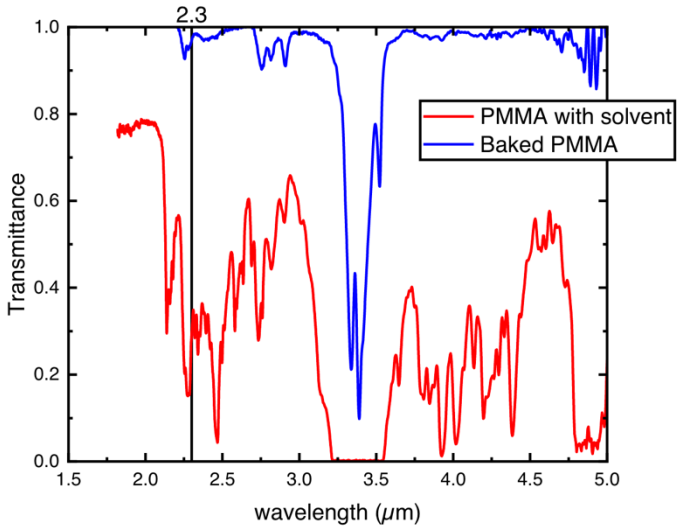

Fig. 2. FTIR measurement of an as-deposited (blue) or baked (red) PMMA drop as a function of the wavelength.

According to the Beer-Lambert law, the transmittance writes:

$$\frac{I}{I_0} = e^{(-\alpha \cdot d)}$$

where d and α are the thickness and the absorption coefficient of the absorbing material, respectively. The thickness of the PMMA measured with a profilometer being d ~1 mm, the absorption coefficient near 2.3 µm was $\alpha \sim 0.3\ cm^{-1}$, i.e. negligible.

The gap of a representative DL/WG pair was filled by simply placing a drop of liquid PMMA on it, and allowing it to seep in for a few minutes before curing it. In this test experiment, PMMA also spilled over the active and passive WGs. Although this is not a problem to study the device, additional processing steps would be required to remove the excess PMMA for large scale fabrication. L-I measurements were then performed by measuring the light output power from the cleaved back mirror and from the exit of the SiN WGs, as in our previous experiments [12]. The results reported in Fig. 3 clearly show the impact of the gap filling. First, the threshold current is

Optics EXPRESS

increased (250 mA) as compared to the air gap case (230 mA), confirming that the PMMA has indeed penetrated through the gap and covered the laser facet. Considering the refractive index of PMMA (1.47), this ~10% threshold increase is perfectly in line with the calculation shown in Fig. 1. In addition, and most important, the total optical transmission through the passive SiN WG is also increased. Given that the exact same device was measured before and after PMMA filling, the large transmission increase can unambiguously be ascribed to an improved coupling efficiency between the active DL and the passive SiN WG.

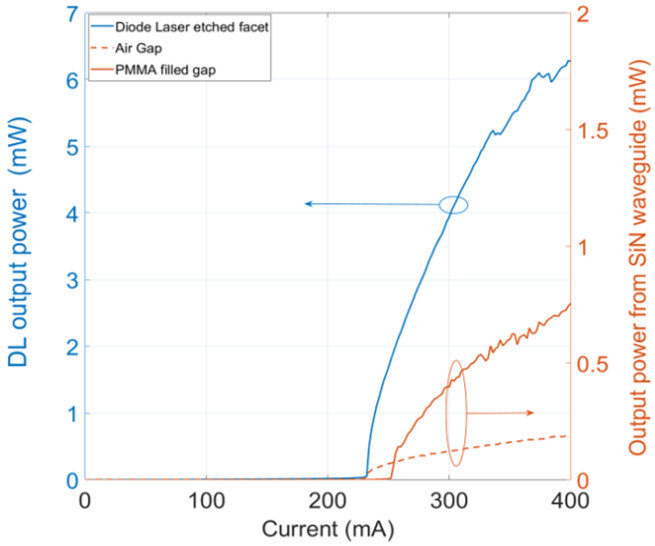

Fig. 3. L-I curves for the Si based PIC device: the blue line refers to the output power collected from the DL back facet; the orange lines represent the output power collected from the SiN waveguide for two different scenarios: the dashed line refers to the case of an air gap, while the solid line refers to the case of gap filled with PMMA.

This shows that a viable strategy to increase the coupling efficiency of butt coupled devices is to fill the gap, as expected from numerical simulations [15]. The threshold current increase could be compensated by depositing high reflectivity coatings on the back facet and/or by increasing the cavity length.

2.2. Improved butt-coupled geometry for monolithically integrated on-chip lasers

A gap-filling strategy was presented in the previous section, showing that the optical coupling can certainly be improved. Based on these results, we propose here an improved butt-coupled geometry, which is achieved by reversing the process flow as compared to Ref. [12–14].

2.2.1. Process flow

In these previous demonstrations, the passive devices were first fabricated on the Si wafers before the growth and processing of the III-V DLs. Here, we propose to first grow the III-V DL on the Si substrate. The III-V stack is then processed to form the facets of the resonant cavity by controlled etching through the entire laser structure (Fig. 4(a)), before depositing a SiO_2 layer of the same thickness as the bottom cladding layer of the laser (Fig. 4(b)). Finally, 800 nm of SiN is deposited as the core layer of the passive waveguide, the same thickness as the III-V gain region (Fig. 4(c)). This allows isolation of the optical mode from the GaSb buffer layer and good alignment between the active and passive waveguides. We expect that during the SiO_2 deposition, a SiO_2 layer will also be deposited on the DL facet, eliminating the air gap and mimicking a scenario similar to

Optics EXPRESS

filling the gap, in this case with SiO_2, whose refractive index is close to that of PMMA used above (See Section 2.1). In the simplified approach studied here, air is used as the upper confinement medium (Fig. 4(c)), but a SiO_2 top cladding layer can also be deposited atop the SiN waveguide to isolate it from the ambient atmosphere. Finally, the SiO_2/SiN stack deposited on top of the III-V heterostructure is etched away to allow processing the III-V material into a DL.

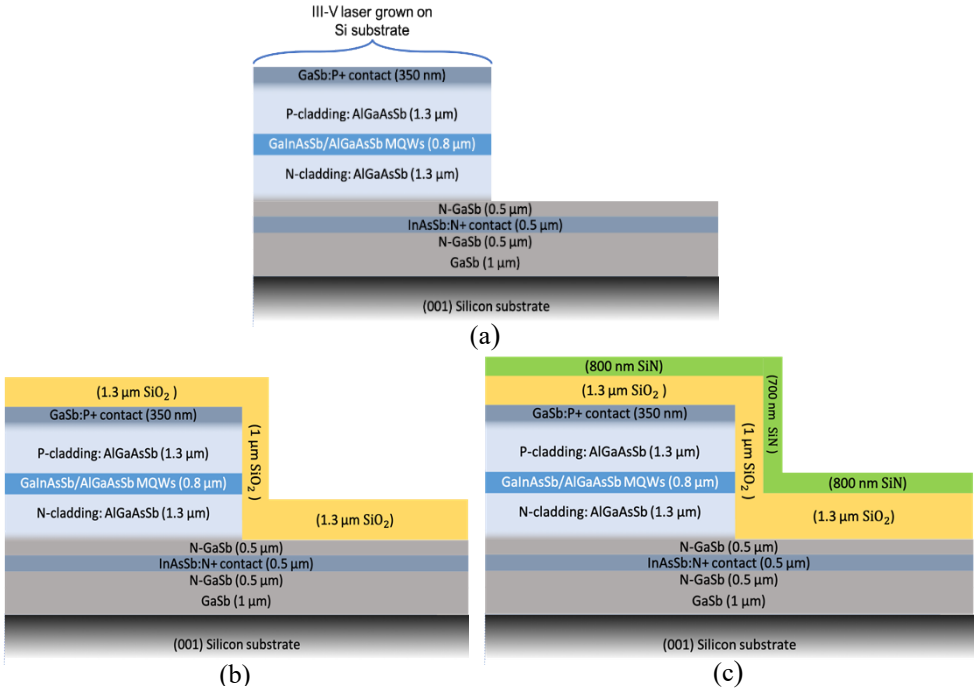

Fig. 4. Sketch of the fabrication process flow: (a) definition of the etched laser cavity, (b) deposition of the SiO_2 bottom cladding layer and (c) final on-chip device obtained after the deposition of 800 nm SiN as WG layer.

2.2.2. FDTD simulations

In order to evaluate the advantages of using the geometry proposed in Fig. 4, the optical coupling was simulated using the Finite Difference Time Domain (FDTD) numerical method, which has been shown to be a robust method for simulating devices as in our case study [15,26,27]. The geometry used in the simulations was based on experimental observations made during preliminary fabrication tests.

Once the active and passive devices have been modelled in 3D, a continuous wave Gaussian beam profile with a wavelength of $\lambda = 2.3\ \mu m$ is used as the input source and it propagates from the active core into the SiN layer of the passive waveguide considered as a lossless material (Fig. 5(a)). Close examination of the optical mode propagation at the active/passive interface shows an efficient light transmission into the passive SiN waveguide, despite the presence of dielectric layers at the interface (Fig. 5(b)). Finally, the monitor plane located at the end of the SiN waveguide provides a transmission value close to 45%, resulting in a several-fold improvement in coupling efficiency as compared to the presence of an air gap [15].

Optics EXPRESS

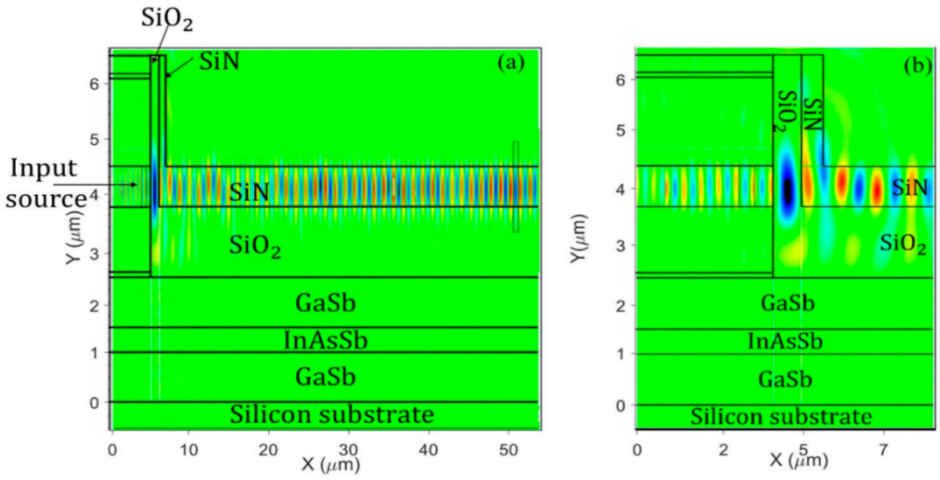

Fig. 5. Contour map of the fundamental TE mode (a) the fundamental TE mode propagates from the active into the passive device based on the optimized butt-coupling configuration; (b) Zoom on the propagation of the optical mode close to the active/passive interface.

3. Device fabrication and characterization

We then fabricated and characterized a device similar to the one described in Fig. 4. For this proof-of-concept we have simplified the approach by using a GaSb DL grown by MBE on a (001) GaSb substrate. This allows us to compare the new DL process with the standard GaSb DL process. The layer stack was similar to that reported in [28] for a DL grown on Si, and the process flow can be easily applied to lasers grown on Si.

The scanning electron microscope (SEM) images shown in Fig. 6 illustrate the main fabrication steps. First, the DL cavity was defined by ICP-RIE dry etching using the approach described in Refs. [24,29]. Vertical facets were obtained, which is crucial for lasing (Fig. 6(a)). The etching was stopped below the n-cladding layer (Fig. 6(b)) to allow a good alignment between the active and passive WGs. A passive bottom cladding layer of 1.7 µm SiO_2 was then deposited by plasma-enhanced chemical vapor deposition (PECVD), resulting in ~1 µm of SiO_2 deposited on the etched facet of the cavity, confirming the absence of any air gap. The next step was to deposit an 800 nm thick SiN layer by PECVD. The deposition rates of SiO_2 and SiN, both deposited at 280°C, were calibrated prior to the device fabrication to control the vertical alignment of the passive SiN WG with the active zone of the DL. A typical uncertainty of 5% on the deposition rate results in a vertical misalignment lower than 100 nm, which, induces negligeable insertion losses. Following the deposition of the full dielectric stack, S-shaped SiN waveguides were defined into the dielectric stack by optical lithography followed by ICP-RIE dry etching stopping at the end of the 800 nm SiN layer (Fig. 6(c)). At this stage, the passive waveguides (10 µm x 2 mm) were fully processed. The dielectric stack lying on top of the laser heterostructure was etched away to process the III-V material. Note that at this stage, the patterned SiN waveguide and the active/passive interface had to be carefully protected, which required special attention to the proper design of the contact lithography masks. This step also ensures the lateral alignment of the active and passive WGs which is not critical given the 10 µm laser ridge width. Finally, 10 x 1.5 mm DLs were fabricated using standard procedures described in [28,29]. The final monolithically integrated on-chip light source butt-coupled to a SiN waveguide is shown in Fig. 6(d).

The sample was then mechanically polished and diced into several bars. Each bar was soldered with the substrate side down to a Cu heatsink for continuous wave (CW) testing at room

Optics EXPRESS

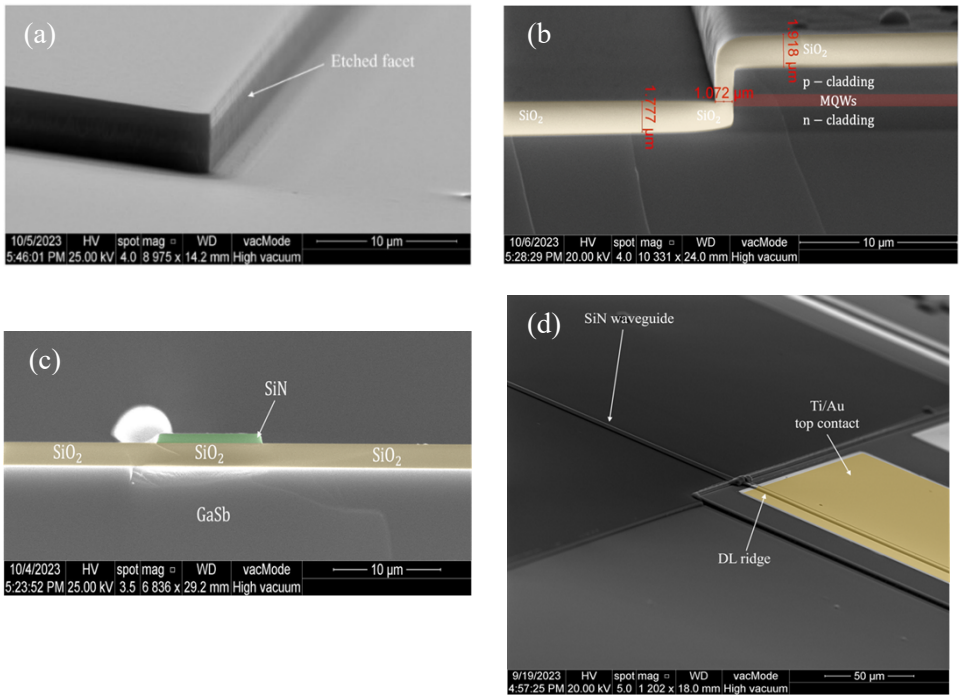

Fig. 6. Scanning Electron Microscope (SEM) pictures: (a) details of the etched facet after definition of the DL cavity, (b) PECVD of 1.7 µm SiO_2 bottom cladding deposited by PECVD. Note that 1 µm SiO_2 was deposited on the laser cavity facet, (c) definition of the passive waveguide after PECVD deposition of 800 nm SiN. The white halo in the background is due to charging effect during the SEM image acquisition. (d) Fully processed monolithically integrated PIC.

temperature on a probe station. Figure 7 shows an optical microscope picture taken from a typical PIC with its GaSb DL coupled to a passive SiN waveguide.

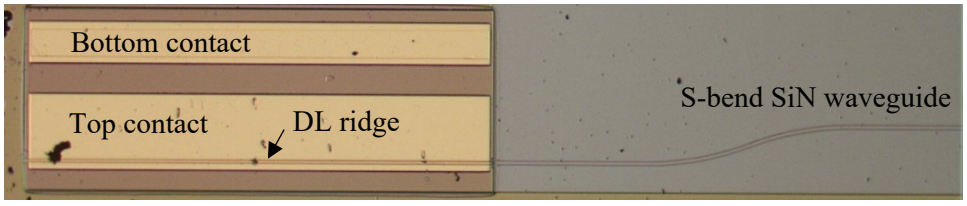

Fig. 7. Optical microscope picture of the final on-chip PIC.

First, we tested the DLs integrated on the PIC and compared their performance with discrete GaSb DLs [30]. L-I-V characteristics were measured from the back-etched facet of the DL in the CW regime using a calibrated power meter and reported in Fig. 8(a). All DLs did lase. The turn-on voltage is around 1.06 V, and the series resistance is close to 6 Ω for all DLs. It should be noted that the threshold current value (42 mA) was slightly increased as compared to DLs on GaSb substrate with as-cleaved facets (~38 mA). This is due to the fact that one facet is coated with a SiO_2/SiN bilayer, which increases the mirror losses, and thus increases the threshold, as shown in Fig. 1.

Optics EXPRESS

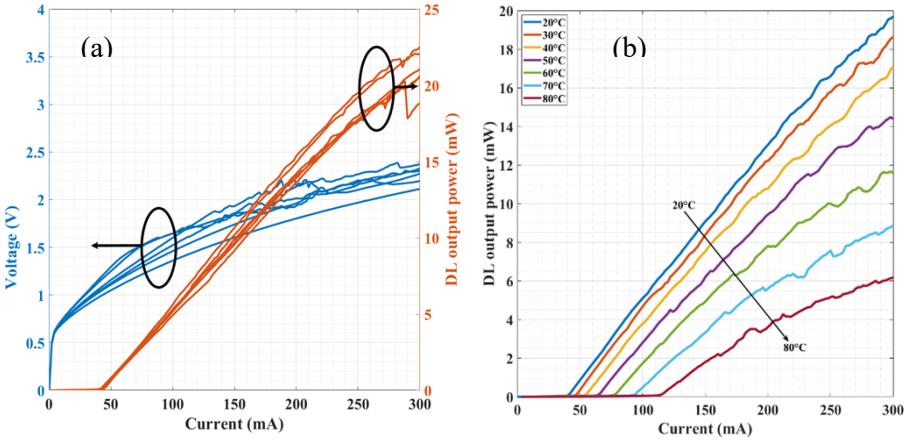

Fig. 8. (a) L-I-V curves taken at room temperature in the CW regime and (b) L-I curves taken at different temperatures between 20°C and 80°C for a typical DL. Both measurements are taken from the back facet of the DL.

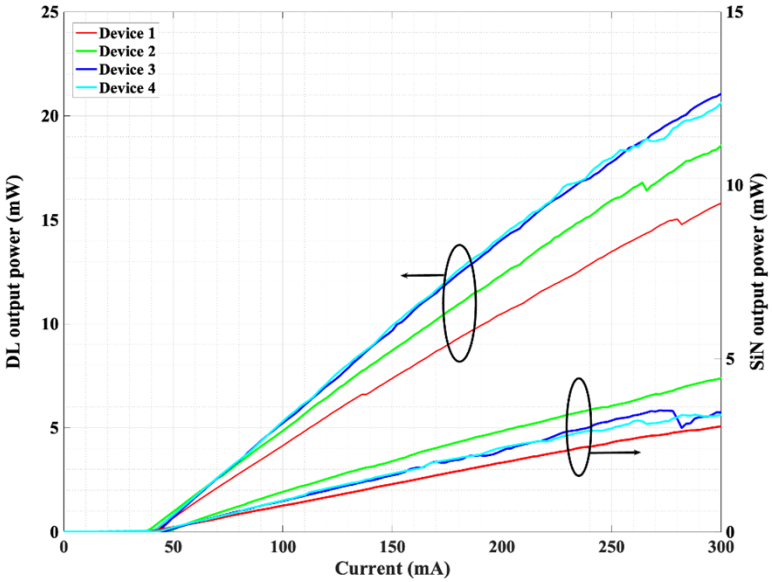

Fig. 9. Comparison of the P-I curves collected from the back-facet of the DL (left axis) and transmitted through the SiN waveguide (right axis).

Figure 8(b) shows the evolution of the *L–I* curves with the measurement temperature between 20 °C and 80 °C (limited by the experimental setup) for a representative DL. Lasing is achieved in the whole temperature range with a threshold current intensity increasing from 42 mA to 114 mA. From this series of experiments, we deduced the corresponding T_0 characteristic temperature, which represents the sensitivity of the laser threshold current to the operating temperature, using the empirical law:

$$I(T)_{th} = I_0 e^{\frac{T}{T_0}}$$

Optics EXPRESS

A T_0 value of 51 K is obtained, in line with typical values for GaSb DLs [30]. The performance of the GaSb DLs thus confirms that processing the dielectric stack after growing the III-V heterostructure did not damage the previously grown DL heterostructure.

The second set of investigations focused on studying the optical transmission by measuring the waveguide output power as a function of the DL drive current. Figure 9 shows the output power from the output facet of the SiN waveguide compared to the DL output power. Both curves show the same threshold current intensity, as expected. From the L-I curves plotted in Fig. 9, we experimentally determine a total light transmission of about 23%. The losses at a wavelength of 2.3 µm for the SiN material used in this experiment have been determined by absorption measurements to be $\sim 2\,\mathrm{cm}^{-1}$, which results in a 67% transmittance through a 2 mm-long WG. Altogether, this means that 35% of the DL light is transmitted through the active/passive interface, which is a 3.5-fold improvement as compared to the situation with an airgap [12], and in reasonable agreement with the 45% simulated value (cf. Section 2.2.2). Additional transmission losses may arise from light scattering on the sidewalls and/or by gas adsorption on the SiN waveguide. This can be alleviated by adjusting the etch parameters to achieve smoother sidewalls, and by cladding the SiN WG with a SiO_2 top layer.

4. Conclusion and perspectives

Although the monolithic integration of active III-V semiconductor lasers and passive Si photonics devices has been demonstrated, improving the optical coupling and reliability remain important challenges. In this work, we have first demonstrated that filling the previously observed airgap [12–14] with a polymer with a refractive index around 1.5 significantly improves light transmission at the active/passive interface. However, this requires additional technology steps after the PICs have been fabricated. To simplify the approach, we have proposed a new strategy to monolithically integrate active III-V lasers and passive dielectric devices, where the passive devices are fabricated after the MBE growth of the III-V semiconductor heterostructure on a planar Si substrate. This naturally suppresses the airgap at the active/passive interface, which is replaced by a thin dielectric interface layer with a refractive index similar to that of the previously studied polymer. With this approach, we have achieved GaSb DLs butt-coupled to SiN passive waveguides with ~23% transmission after 2 mm SiN. Taking into account the losses of the SiN waveguide, this translates into a 35% transmission at the interface, in reasonable agreement with the value simulated by FDTD, which represents a 3.5 fold improvement as compared to previous results. The total transmittance could further be increased cladding the SiN waveguide with **SiO_2**. In addition, the coupling efficiency could be increased by using anti-reflection subwavelength gratings on the input facet of the waveguide or using of a taper [31]. A solution to increase the transmitted power at constant coupling efficiency is to use a high-reflection coating on the back facet of the laser. Altogether, this strategy paves the way for an optimized route to monolithically integrate active and passive photonic devices with a high light coupling efficiency.

Funding. Agence Nationale de la Recherche (Equipex EXTRA ANR-11-EQPX-0016, Project LightUp ANR-19-CE24-0002); H2020 Marie Skłodowska-Curie Actions (860808, OPTAPHI); H2020 Excellent Science (780240, Redfinch).

Disclosures. The authors declare no conflict of interest.

Data availability. Data underlying the results presented in this paper are not publicly available at this time but may be obtained from the authors upon reasonable request.

References

1. V. M. N. Passaro, C. D. Tullio, B. Troia, *et al.*, "Recent Advances in Integrated Photonic Sensors," Sensors **12**(11), 15558–15598 (2012).
2. J. Song, X. Luo, J. S. Kee, *et al.*, "Silicon-based optoelectronic integrated circuit for label-free bio/chemical sensor," Opt. Express **21**(15), 17931–17940 (2013).
3. D. Liang and J. E. Bowers, "Recent progress in lasers on silicon," Nat. Photonics **4**(8), 511–517 (2010).
4. Z. Zhou, X. Ou, Y. Fang, *et al.*, "Prospects and applications of on-chip lasers," eLight **3**(1), 1 (2023).

Optics EXPRESS

5. A. Spott, E. J. Stanton, A. Torres, *et al.*, "Interband cascade laser on silicon," Optica **5**(8), 996–1005 (2018).
6. A. Spott, J. Peters, M. L. Davenport, *et al.*, "Quantum cascade laser on silicon," Optica **3**(5), 545–551 (2016).
7. A. W. Fang, H. Park, O. Cohen, *et al.*, "Electrically pumped hybrid AlGaInAs-silicon evanescent laser," Opt. Express **14**(20), 9203–9210 (2006).
8. G. Roelkens, J. Zhang, L. Bogaert, *et al.*, "Present and future of micro-transfer printing for heterogeneous photonic integrated circuits," APL Photonics **9**(1), 010901 (2024).
9. E. Tournié, L. Monge Bartolome, M. Rio Calvo, *et al.*, "Mid-infrared III–V semiconductor lasers epitaxially grown on Si substrates," Light: Sci. Appl. **11**(1), 165 (2022).
10. A. Gilbert, M. Ramonda, L. Cerutti, *et al.*, "Epitaxial Growth of III-Vs on On-Axis Si: Breaking the Symmetry for Antiphase Domains Control and Burying," Adv. Opt. Mater. **11**(15), 2203050 (2023).
11. J.-S. Park, M. Tang, S. Chen, *et al.*, "Heteroepitaxial Growth of III-V Semiconductors on Silicon," Crystals **10**(12), 1163 (2020).
12. A. Remis, L. Monge-Bartolome, M. Paparella, *et al.*, "Unlocking the monolithic integration scenario: optical coupling between GaSb diode lasers epitaxially grown on patterned Si substrates and passive SiN waveguides," Light: Sci. Appl. **12**(1), 150 (2023).
13. W.-Q. Wei, A. He, B. Yang, *et al.*, "Monolithic integration of embedded III-V lasers on SOI," Light: Sci. Appl. **12**(1), 84 (2023).
14. K. Feng, C. Shang, E. Hughes, *et al.*, "Quantum Dot Lasers Directly Grown on 300 mm Si Wafers: Planar and In-Pocket," Photonics **10**(5), 534 (2023).
15. M. Paparella, L. M. Bartolome, J.-B. Rodriguez, *et al.*, "Analysis of the Optical Coupling Between GaSb Diode Lasers and Passive Waveguides: A Step Toward Monolithic Integration on Si Platforms," IEEE Photonics J. **14**(5), 1–6 (2022).
16. R. Koscica, C. Shang, K. Feng, *et al.*, "Impact of Pocket Geometry on Quantum Dot Lasers Grown on Silicon Wafers," Adv. Photonics Res. **5**(3), 2300317 (2024).
17. F. Gardes, A. Shooa, G. De Paoli, *et al.*, "A Review of Capabilities and Scope for Hybrid Integration Offered by Silicon-Nitride-Based Photonic Integrated Circuits," Sensors **22**(11), 4227 (2022).
18. S. Iadanza, A. P. Bakoz, P. K. J. Singaravelu, *et al.*, "Thermally stable hybrid cavity laser based on silicon nitride gratings," Appl. Opt. **57**(22), E218–E223 (2018).
19. S. Iadanza, J. H. Mendoza-Castro, T. Oliveira, *et al.*, "High-Q asymmetrically cladded silicon nitride 1D photonic crystals cavities and hybrid external cavity lasers for sensing in air and liquids," Nanophotonics **11**(18), 4183–4196 (2022).
20. G. Ricchiuti, A. Walsh, J. H. Mendoza-Castro, *et al.*, "Photothermal spectroscopy on-chip sensor for the measurement of a PMMA film using a silicon nitride micro-ring resonator and an external cavity quantum cascade laser," Nanophotonics **13**(13), 2417–2427 (2024).
21. "Beam Optics," in *Fundamentals of Photonics* (John Wiley & Sons, Ltd, 1991), pp. 80–107.
22. "A Phenomenological Approach to Diode Lasers," in *Diode Lasers and Photonic Integrated Circuits* (John Wiley & Sons, Ltd, 2012), pp. 45–90.
23. A. Remis, L. Monge-Bartolomé, G. Boissier, *et al.*, "Effect of dislocations on the performance of GaSb-based diode lasers grown on silicon," J. Appl. Phys. **133**(9), 093103 (2023).
24. A. Remis, *Integration of mid-IR lasers on silicon photonic integrated circuits*, (University of Montpellier, 2023).
25. X. Zhang, J. Qiu, J. Zhao, *et al.*, "Complex refractive indices measurements of polymers in infrared bands," J. Quant. Spectrosc. Radiat. Transfer **252**, 107063 (2020).
26. R. M. Joseph and A. Taflove, "FDTD Maxwell's equations models for nonlinear electrodynamics and optics," IEEE Trans. Antennas Propag. **45**(3), 364–374 (1997).
27. K. Yee, "Numerical solution of initial boundary value problems involving maxwell's equations in isotropic media," IEEE Trans. Antennas Propag. **14**(3), 302–307 (1966).
28. M. Rio Calvo, L. Monge Bartolomé, M. Bahriz, *et al.*, "Mid-infrared laser diodes epitaxially grown on on-axis (001) silicon," Optica **7**(4), 263–266 (2020).
29. L. Monge-Bartolome, T. Cerba, D. A. Díaz-Thomas, *et al.*, "Etched-cavity GaSb laser diodes on a MOVPE GaSb-on-Si template," Opt. Express **28**(14), 20785–20793 (2020).
30. G. Belenky, L. Shterengas, M. V. Kisin, *et al.*, "Gallium antimonide (GaSb)-based type-I quantum well diode lasers: recent development and prospects," in *Semiconductor Lasers*, A. Baranov and E. Tournié, eds., Woodhead Publishing Series in Electronic and Optical Materials (Woodhead Publishing, 2013), pp. 441–486.
31. L. Puts, X. Leijtens, P. Cheben, *et al.*, "Anti-reflection subwavelength gratings for InP-based waveguide facets," Opt. Lett. **46**(15), 3701–3704 (2021).